Hg/Molecular Monolayer−Si Junctions: Electrical Interplay between Monolayer Properties and Semiconductor Doping Density

Omer Yaffe,[†,‡] Luc Scheres,[†,§] Lior Segev,[‡] Ariel Biller,[‡] Izhar Ron,[‡] Eric Salomon,[||] Marcel Giesbers,[§] Antoine Kahn,[||] Leeor Kronik,[‡] Han Zuilhof,[§] Ayelet Vilan,*[,‡] and David Cahen*[,‡]

Department of Materials and Interfaces, Weizmann Institute of Science, Rehovot 76100, Israel, Laboratory of Organic Chemistry, Wageningen University, Dreijenplein 8, 6703 HB Wageningen, The Netherlands, and Department of Electrical Engineering, Princeton University, Princeton, New Jersey, 08544

Received: February 24, 2010; Revised Manuscript Received: April 29, 2010

Metal−organic molecule−semiconductor junctions are controlled not only by the molecular properties, as in metal−organic molecule−metal junctions, but also by effects of the molecular dipole, the dipolar molecule−semiconductor link, and molecule−semiconductor charge transfer, and by the effects of all these on the semiconductor depletion layer (i.e., on the internal semiconductor barrier to charge transport). Here, we report on and compare the electrical properties (current−voltage, capacitance−voltage, and work function) of large area Hg/organic monolayer-Si junctions with alkyl and alkenyl monolayers on moderately and highly doped n-Si, and combine the experimental data with simulations of charge transport and electronic structure calculations. We show that, for moderately doped Si, the internal semiconductor barrier completely controls transport and the attached molecules influence the transport of such junctions only in that they drive the Si into inversion. The resulting minority carrier-controlled junction is not sensitive to molecular changes in the organic monolayer at reverse and low forward bias and is controlled by series resistance at higher forward bias. However, in the case of highly doped Si, the internal barrier is smaller, and as a result, the charge transport properties of the junction are affected by changing from an alkyl to an alkenyl monolayer. We propose that the double bond near the surface primarily increases the coupling between the organic monolayer and the Si, which increases the current density at a given bias by increasing the contact conductance.

Introduction

Incorporating molecular elements into electronic devices poses a fascinating scientific challenge.[1] By varying the molecular chemistry, we hope to tailor the device's electrical properties, possibly leading to flexible and scalable fabrication schemes. Much of the work in this direction focuses on single molecules or monolayer ensembles on metal electrodes.[2−4] Using a semiconductor instead of a metal provides significant physical and technological advantages,[5−9] among which are possibly tunable interactions between the semiconductor bands and the molecular energy levels that may lead to novel electrical behavior.[5] Semiconductor (SC) surfaces, as well as metal ones, can be functionalized with organic molecules to yield stable and high-quality monolayers.[10−13] However, unlike metals, the bulk electronic properties of semiconductors can be tailored through doping and the (near-)surface properties can be modified via electrical dipoles and (monopole) charges, thereby considerably expanding the possibilities for tuning the device performance.[14,15]

Adsorbing molecules on the SC surface generally changes the surface potential and, thus, the SC work function (and electron affinity).[16] This potential change at the SC surface can extend from roughly a few nanometers to a few micrometers into the semiconductor, forming a space charge region (SCR), which constitutes an internal barrier for charge transport. Therefore, if a metal contact is made to the SC, the presence of molecules at the interface can change the internal charge transport barrier across the resulting junction.[9,17] This internal SC barrier changes the current−voltage ($J-V$) characteristics of the junction, in addition to the specific charge transport barrier imposed by the molecules. Hence, the "molecular effect" of hybrid metal/organic molecule/semiconductor (MOMS) junctions can be divided into (a) the overall dipole of the molecules on the surface, plus any molecule−substrate charge transfer that affects the effective SC electron affinity; (b) the electronic transport barrier, presented by the molecules, especially if they form a continuous monolayer.

In addition, the introduction of surface/interface states can also have a large effect on the electrical properties of the junction. However, it was shown in the past that the interface state density of well-prepared Si−organic monolayer interfaces is very low.[18,19]

The doping density of the SC affects the relative importance of effects (a) and (b), because an increase in doping density can (1) induce image charge lowering of the barrier, (2) decrease the SC depletion layer width[20,21] and, thereby, increase the probability of tunneling through the SCR barrier (field emission), and (3) affect the magnitude of the surface dipole, induced by the monolayer.[22] Therefore, the molecular properties (e.g., degree of conjugation, presence of redox active centers, molecular length) will have different overall effects for different doping levels of otherwise identical semiconductors.

To study and comprehend this interplay between the molecular and Si properties, we compare here the electrical charac-

* Author for correspondence. E-mail david.cahen@weizmann.ac.il.
† These authors contributed equally to this work.
‡ Weizmann Institute of Science.
§ Wageningen University.
|| Princeton University.

10.1021/jp101656t
Published on Web 05/13/2010

Figure 1. Schematic representation of the alkyl (left) and alkenyl (right) molecule on n-Si(111). R represents a methyl-terminated alkyl chain with a length varying between 10 and 16 carbons.

teristics of Hg/monolayer−Si junctions with alkyl and alkenyl monolayers on n-Si(111) (see Figure 1), where saturated alkene-derived monolayers are referred to as "alkyl" and unsaturated alkyne-derived ones as "alkenyl". Both types of monolayer were formed on moderately and highly doped n-Si(111), with $N_d \approx 10^{15}$ cm^{-3} (labeled MD) and 10^{19} cm^{-3} (labeled HD), respectively. This choice for a test system is convenient, because Hg has proven to be an efficient "soft", nondestructive top contact for molecular electronics,[23−25] and both alkyl and alkenyl monolayers were shown to be densely packed and with good chemical passivation properties.[26,27] This behavior then allows us to examine the extent to which a minor difference such as one double bond in a long alkyl chain can change the overall electrical transport properties of such junctions.

We find clear differences between $J-V$ characteristics of MOMS on MD and HD n-Si(111). Furthermore, while the $J-V$ characteristics of alkyl and alkenyl-based MOMS are almost identical for MOMS on MD Si, they differ for those on HD Si.

Experimental and Computational Details

Sample Preparation. Single side polished n-type Si(111) wafers with a nominal resistivity of 1−10 Ω−cm (MD Si, $N_d \approx 10^{15}$ cm^{-3}) and 0.006 Ω−cm (HD Si, $N_d \approx 10^{19}$ cm^{-3}) were purchased from Siltronix (France). Sample preparation and characterization followed literature descriptions.[12,27] Briefly, pieces of Si wafer were cleaned by sonication in acetone and oxidized by an oxygen plasma (Harrick PDC-002 setup) for 3 min. Subsequently, the Si(111) substrates were etched in an argon-saturated 40% NH_4F solution for 15 min. After etching, the samples were rinsed with water, blown dry with nitrogen, and immersed in argon-saturated neat 1-alkyne or 1-alkene (GC purity >99.9%) at 120 °C and ∼10 mbar. After 16 h, the reaction was stopped and the monolayers were rinsed extensively with PE40/60,[28] EtOH, and CH_2Cl_2 and sonicated for 5 min in CH_2Cl_2 to remove physisorbed molecules. For MD Si, the examined monolayers were made with molecules with chain lengths of 12, 16, and 18 carbons, while for HD Si, the molecules had chain lengths of 14, 16, and 18 carbons. This mismatch is due to the varying quality of the precursor molecules that were available at given times. $J-V$ measurements were performed on n-Si/monolayer/Hg junctions, formed by placing a Hg (99.9999% purity) drop on the monolayer, using a controlled growth hanging mercury drop (HMD) electrode (Polish Academy of Sciences, Poland). The samples were contacted on the back by applying In−Ga eutectic, after scratching the surface with a diamond knife. Measurements were carried out in a controlled environment glovebox with 10% relative humidity. The contact area between the Hg drop and the monolayer (typically 0.6 mm in diameter) was determined using an optical microscope.

Current−Voltage. $J-V$ measurements were done with a Keithley 6430 sub-fA current/voltage source-measure unit. Several scans from −1 to 2 V (applied to Hg) were measured for each junction with a scan rate of 20 mV/s. At least 7 junctions were made on each sample, and the results represent the average of all the measurements. None of the measurements was rejected. Impedance measurements were performed with an HP4284A precision LCR meter. The ac amplitude was 10 mV, and the measurement frequency was 500 kHz. This frequency was sufficiently high to prevent quasi-static behavior and prevent possible interface states from following the ac signal. The impedance model used for the $J-V$ measurements was a parallel circuit of a resistor and capacitor, commonly used to characterize such monolayers.[17,18]

Contact Potential Difference. CPD measurements were performed with a custom-made Kelvin Probe setup, based on a commercial Besocke Delta Phi Kelvin probe + controller, which are placed in a glovebox with controlled 10% relative humidity. The surface potential of the monolayers was measured, relative to that of a vibrating Au grid that was calibrated prior to the measurements against freshly peeled highly ordered pyrolytic graphite (HOPG).

X-ray Photoelectron Spectroscopy. XPS analyses were performed using a JPS-9200 photoelectron spectrometer (JEOL, Japan). High-resolution spectra were obtained under UHV conditions using monochromatic Al Kα X-ray radiation at 12 kV and 25 mA, using an analyzer pass energy of 10 eV. All high-resolution spectra were corrected with a linear background before fitting.

Infrared Reflection−Absorption. IRRA spectra were collected with a Bruker spectrometer (model Tensor 27), equipped with a liquid N_2-cooled MCT detector and a variable-angle reflection accessory (AutoSeagull). A Harrick grid polarizer was placed in front of the sample for measuring spectra with p-polarized (parallel) light. In order to get the optimal signal-to-noise ratio on HD n-Si, the variable-angle reflection accessory was set to 50°, i.e., the incoming light makes an angle of 50° with respect to the surface normal.[29] The spectra were taken by adding 2048 scans at a resolution of 2 cm^{-1} and referenced to a clean native oxide-covered Si sample without further data manipulation.

Ultraviolet Photoemission Spectroscopy. UPS experiments involved detailed measurements of the valence states of the monolayer-covered Si, including the photoemission cutoff, from which the vacuum level position and the work function are determined. HeI (21.22 eV) and HeII (40.8 eV) radiation lines were used for these experiments. The methodology followed for these measurements has been described elsewhere.[14] Band bending in the Si substrate, prior to the formation of a metal contact, was extracted from XPS scans of the Si_{2p} core level and from previous knowledge of the energy difference between the core level and the top of the Si valence band.

Atomic Force Microscopy. AFM was performed in the tapping mode (ac), using a Nanoscope V Multimode AFM (Veeco, USA) and standard Si probes (OMCL-AC240TS-W2, Olympus, Japan). Typical peak forces were around 5 nN; typical scan rates were 1−2 Hz.

Device Numerical Simulations. Simulations were based on the approach of Tarr et al.[30] for ultrathin insulator MIS devices. In essence, the algorithm solves self-consistently both the total potential drop over the device and the total current density supported by it. The framework is that of a p^+-n junction, with charge carrier transport across it suppressed by tunneling. Following ref 26, tunneling can be approximated by a WKB-based integral, attributing a band structure to the monolayer. This simplified approach can produce hole currents within 20%

TABLE 1: Ellipsometric Thicknesses (*d*) and Static Water Contact Angle (CA) of Alkyl and Alkenyl Monolayers on HD n-Si(111)

	ellipsometry *d* (Å ± 1 Å)		static water contact angle θ (° ± 1°)	
number of carbons	alkyl	alkenyl	alkyl	alkenyl
14	16	15	107	107
16	19	20	110	111
18	20	21	108	109

of the experimental data, which is sufficiently accurate for our purposes. Semiconductor and metal parameters used in the simulations are given in Table 1 of the Supporting Information. The monolayer was modeled as a wide band gap insulator (E_g = 7.3 eV as experimentally measured for alkenes)[14] with a dielectric constant of 2.

Electronic Structure Calculations. Calculations were performed for octyl and octenyl chains bound to Si(111), as shown in Figure 1. A (2 × 1) surface structure, with alkyl chains attached to one of the two surface Si atoms, was used. Dangling surface Si bonds were passivated by H atoms. The double bond was placed between the carbon atoms closest and second closest to the Si surface. All calculations were performed within a three-dimensional periodic super cell, using a symmetric slab configuration. This guarantees that the structure is devoid of a net dipole perpendicular to the Si-molecule interface, which would be inconsistent with the periodic boundary condition.[31,32] All calculations were performed with twelve atomic layers of silicon and a vacuum region equivalent to ten atomic layers of silicon. These values were found to be sufficient for a well-converged calculation that mimics a surface-terminated material. The electronic structure was determined by solving the Kohn−Sham equations of density functional theory, using the plane wave approach as implemented in the Vienna ab initio simulation package (VASP).[33] The local density approximation (LDA)[34] that was previously shown to be sufficient for describing the electronic structure of alkyl chains on Si,[35−37] was employed for the exchange-correlation functional. Surface dipole changes were computed by calculating the average electrostatic potential from the electronic charge density and nuclear coordinates along the direction perpendicular to the surface.[32] Specifically, we compared the potential difference between the vacuum region and a local maximum point found in the middle of the slab of the reference system, for an alkyl and alkenyl monolayer structure.[35]

For interpretation of XPS data, additional computations of the charge distribution within the organic chain were performed using B3LYP/6-311G(d,p) calculations with the *Gaussian 09* (rev A2) suite of programs. For technical reasons, a $(SiH_3)_3Si$ cluster (rather than a Si slab) was used in the simulation, to which either an alkyl or an alkenyl chain was attached (several lengths—C_4 was shortest). To properly compare the charges on the sp^2-hybridized C (underscore marks the carbon that charge density was computed for) in Si—C═C and the sp^3-hybridized C in Si—C—C, light-in-heavy charges were used, in which the charge of the attached H atoms was added to that of the C atom.[38]

Results and Discussion

Monolayer Characterization. The structural quality of a monolayer is a very important issue when studying the electrical properties of organic monolayers linked to Si.[18,26,39] Therefore, prior to the electrical measurements, the quality of all organic monolayers was studied in detail. Because one characterization method is insufficient to determine that the monolayers are densely packed and of high quality, a combination of static water contact angle (CA) measurements, ellipsometry, infrared spectroscopy (ATR-IR or IRRAS), and X-ray photoelectron spectroscopy (XPS) was used in this study. The preparation of high-quality (in terms of carbon density, homogeneity, and chemical passivation of the Si surface) alkyl and alkenyl monolayers on MD n-Si(111) has been reported,[12,26,27] and we refer to references for details of the characterization that we performed on the monolayers that we used. Because only lower-quality monolayers have been reported on HD n-Si(111),[15,40] we report here on their characterization. Table 1 summarizes the static contact angles (θ) and the ellipsometric thicknesses (*d*) of all alkyl and alkenyl monolayers on HD n-Si(111).

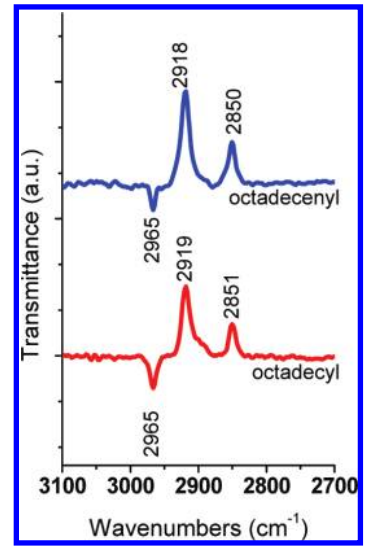

Figure 2. IRRA spectra (p-polarization) of octadecyl (bottom, red) and octadecenyl (top, blue) monolayers on HD n-Si(111).

The range of measured CA is well above the 102°−104° reported before on Si with identical doping level[15] and close to the 110°−111° that has been reported for monolayers on MD n-Si.[14,18,27] This indicates that these alkyl and alkenyl monolayers on HD n-Si(111) are of a quality comparable to those on MD n-Si(111). Furthermore, the thickness of these alkyl and alkenyl monolayers on HD n-Si(111) agrees well with the values reported for these monolayers on MD n-Si(111).[26,27] Although the thickness increase from C_{16} to C_{18} is smaller than expected, the differences compared to the C_{16} and C_{18} monolayers on MD n-Si(111) are still within experimental error (±1 Å).

In addition, IRRAS was used to analyze the alkyl and alkenyl monolayers on HD n-Si(111). Spectra of the octadecyl and octadecenyl monolayers on HD n-Si(111) are shown in Figure 2. We note that, because on HD n-Si(111) we measured the external reflection of the p-polarized light at an incidence angle of 50° with respect to the surface normal, the resulting IRRA spectra exhibit positive peaks for the antisymmetric and symmetric methylene stretching vibrations ($\nu_a(CH_2)$ and $\nu_s(CH_2)$), respectively, and a negative peak for the antisymmetric methyl stretching vibration ($\nu_a(CH_3)$).[15,29] The position of $\nu_a(CH_2)$ is commonly used as an indicator of the intermolecular environment of the organic chains. Values of 2919−2920 cm^{-1} are typical for crystalline, solid alkanes, and 2926−2928 cm^{-1} values characterize liquid, isotropic alkanes. For the octadecyl and octadecenyl monolayers on HD n-Si(111), the $\nu_a(CH_2)$ and $\nu_s(CH_2)$ peaks were detected at 2919 and 2851 cm^{-1} and at 2918 and 2850 cm^{-1}, respectively, indicating that both monolayers

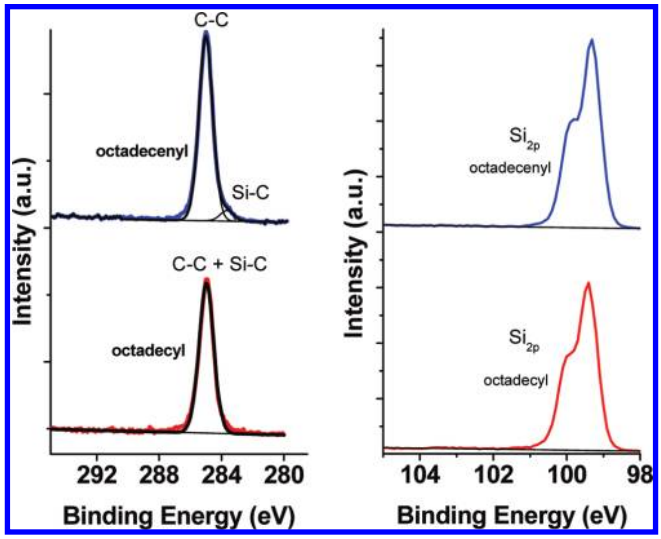

Figure 3. High-resolution XPS C_{1s} and Si_{2p} narrow scans of 1-octadecyl (bottom, red) and 1-octadecenyl (top, blue) monolayers on HD n-Si(111).

on HD n-Si(111) are densely packed.[41,42] In a previous report, it was also shown that, in the case of alkenyl monolayers on MD Si, there is a peak at 1602.8 cm^{-1}, which is assigned to the C═C vibration mode.[27] This peak was not observed for the same monolayer on HD Si, probably because only IRRA spectroscopy can be used for HD Si, while in the case of MD, the ATR-IR technique that was (and could be) used is significantly more sensitive than the former.

As shown in Figure 3, the XPS C_{1s} narrow scans show the different linkage of the two monolayers to the HD n-Si(111). For the 1-octadecyl monolayer, the energy of the C_{1s} electrons from the silicon-bound carbon (Si−C) is very close to that of the aliphatic carbons, and therefore, the narrow scan consists of only one main peak at ~285.0 eV. In contrast, the C_{1s} peak of the octadecenyl monolayer can be deconvoluted into two contributions, as the carbon, bound to the relatively electropositive Si, shifts to ~283.5 eV. The higher electron density on the Si−C═C carbon present in the alkenyl chain shifts the emission peak in comparison to the Si−C−C carbon present in the alkyl chain. Furthermore, the ratio of peak areas between the small 283.5 eV peak and the large 285.0 eV peak is 0.73/17. Taking into account the attenuation of the 283.5 eV peak due to the buried nature of the Si−C═C atom, the theoretically expected ratio would have been 0.75/17.[27,43] As a result, the ratio of the Si−C═C/other C atoms is 1/17, which agrees with the ratio of the one C bound to the Si and the number of C atoms, remaining in the total C18 chain. This is also borne out by the natural population charge calculations on $(SiH_3)_3Si$−organic chain clusters, in which the organic chain was at least four carbon atoms long (butyl or butenyl). The results with chains longer than four carbons were essentially the same as those for the four carbon chains. For the Si−C═C carbon, the light-in-heavy charge was calculated to be −0.42, while for the Si−C−C carbon, this was −0.37. Such a difference is consistent with the positions of the minor peak in the XPS-measured C_{1s} binding energies. This shift might also indicate differences in the interaction between the attached organic chain and the Si substrate, as discussed below.

We note that the XPS Si_{2p} narrow scans of both monolayers did not show any traces of oxidized Si around 103−104 eV,[12,26,27] an important criterion when studying electrical properties of organic monolayer−Si systems.

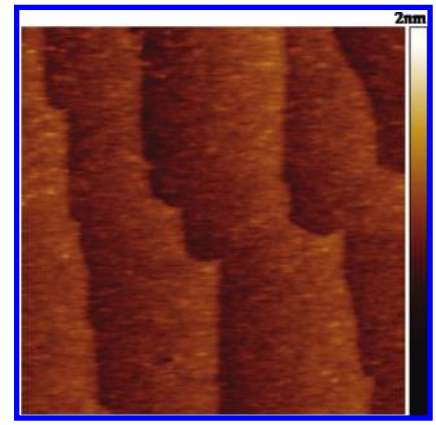

Figure 4. AFM topography (400 × 400 nm^2) of an octadecyl monolayer on HD n-Si(111). Note that the monolayer topography reproduces the typical topography of the H-terminated Si(111) surface, after etching in NH_4F.[44,45]

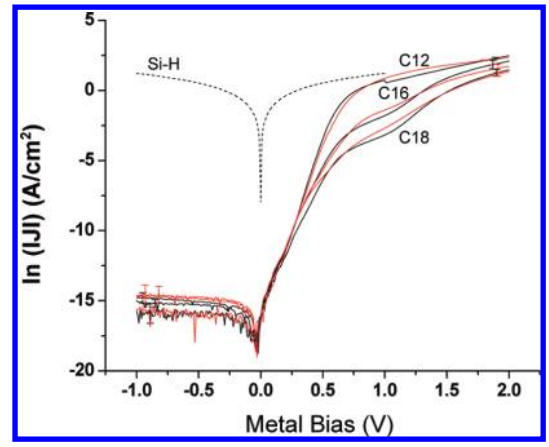

Figure 5. ln(|*J*|)−*V* curves of MD n-Si/organic molecular monolayer/Hg of 12, 16, and 18 carbon chain alkyl (black) and alkenyl (red) monolayers, together with the ln(*J*)−*V* curve of a freshly etched Si−H MOMS (dashed). Bias is applied to the Hg, and the Si is grounded. Scan rate: 20 mV/s. Results are logarithmic averages of at least 7 different junctions. The error bars represent the standard deviations, which are typically less than 5% of the measured current.

Finally, AFM (Figure 4) shows that the topography of the octadecene-derived monolayer reproduces the typical features of the underlying H−Si(111) surface,[44,45] indicating that these monolayers on HD-n-Si are smooth and dense, which was not the case for previously reported ones on HD n-Si(111).[15] All the above data clearly demonstrate that high-quality alkyl and alkenyl monolayers were prepared on HD n-S(111), with contact angles, widths, and densities comparable to those of alkyl and alkenyl monolayers on MD n-Si(111).[27] However, as shown earlier,[26] the most sensitive indication of monolayer quality is the current−voltage behavior of the MOMS, which is the primary subject of this report.

Electrical Properties of MOMS Junctions on MD Si. Figure 5 shows the ln(|*J*|)−*V* curves of MD n-Si/monolayer/Hg junctions with both alkyl (black) and alkenyl (red) monolayers of three different chain lengths (12, 16, and 18 carbon chains). For reference, the dashed line shows the current−voltage behavior of a Si−H/Hg junction, which is ohmic and symmetric, i.e., currents are linear with bias. For the MOMS structures, it is clear that there are two distinct bias ranges, as predicted by numerical simulations[46] and shown experimentally.[8]

In agreement with earlier studies,[8,9] the reverse and low forward bias characteristics of the different MOMS structures on MD n-Si are indistinguishable, within experimental error (but

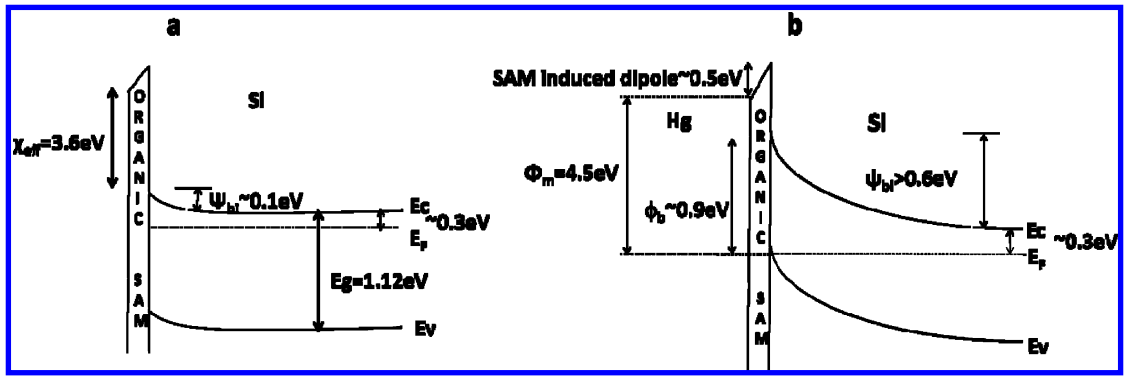

Figure 6. Band diagrams of organic monolayer/MD n-Si structure before (left) and after (right) contact with Hg, where χ_{eff} is the effective electron affinity (measured), Ψ_{bi} is the built-in potential, measured as band bending, ϕ_b is the barrier for transport (calculated), E_g is the Si band gap, and Φ_m is the Hg work function.[56]

clearly different from the H−Si one). This range is denoted as the "semiconductor-limited" regime.[46] At higher forward bias, both the chain length and the type of monolayer (i.e., alkyl or alkenyl) affect the magnitude and shape of the current density curve. We now discuss these two regimes and the effect of series resistance on the latter.

Reverse and Low Forward Bias Range. The SC internal barrier of an ideal junction between a noninteracting metal and semiconductor can be calculated from

$$\phi_b = \Phi_m - \chi_{eff} \quad (1)$$

which represents the Schottky limit.[21] Here, any change in the effective electron affinity (χ_{eff})[47] of the SC directly affects the barrier to transport in the SC (ϕ_b) for a given metal work function (Φ_m).[48]

However, metal−Si Schottky diodes usually exhibit Fermi level pinning, yielding a barrier height that is lower or higher than predicted.[49] The presence of an ultrathin insulating layer (such as our dense organic monolayers) can prevent metal−Si chemical interactions and, if the Si surface is well-passivated, make the junction behave as an ideal one.[9,48]Furthermore, it is known that no Fermi level pinning occurs in the case of a Si−H/Hg junction.[50] Therefore, that junction should follow the Schottky equation (eq 1) and the effective electron affinity of a given surface can be used in eq 1 to estimate ϕ_b. From UPS measurements, a H−Si work function of 4.39 eV is derived, corresponding to an effective electron affinity of 4.15 eV, which agrees with the values of 4.17−4.23 eV reported earlier.[51] By using eq 1 and $\phi_{Hg} = 4.49$eV, the ϕ_b for ideal Hg/H−Si(n) contacts is estimated to be 0.34 eV. Such a low internal barrier is usually negligible if measurements are performed at room temperature[17] and is consistent with the experimentally observed ohmic behavior of the Si:H/Hg junction (Figure 5).

The effective electron affinity of Si-monolayer samples was extracted from UPS and CPD measurements. Both methods gave similar results. The work function of all examined samples on MD n-Si(111) was 3.9 ± 0.1 eV, irrespective of chain length or monolayer type. This ~0.5 eV reduction in work function compared to that for Si−H (with a work function of 4.39 eV) is ascribed to the interfacial dipole of the adsorbed molecules, as discussed elsewhere.[16,35,52−54] From the position of the XPS Si_{2p} peak, a band bending of 0.06 eV was deduced. Because ($E_v - E_F$) is about 0.8 eV, the effective electron affinity is 3.6 ± 0.1 eV.[47,55] The independence of the measured electron affinity on the chain length is not surprising. It was shown in the past that the overall change in surface dipole of a given surface, due to the adsorption of an organic monolayer, is a sum of the surface−molecule bond dipole and dipole of the molecule before adsorption.[35,52] Hence, an additional CH_2 group in the middle of the chain should not have any effect on the interface dipole, because it does not change the molecular dipole. However, what is surprising is that we do not find a difference between alkyl and alkenyl monolayers, because there are differences in the average tilt angle in the monolayer, the molecular dipole of the isolated molecules and in the overall coverage of the atop Si atoms (~50% for alkyl and ~65% for alkenyl).[27] Furthermore, the presence of the double bond adjacent to the Si surface (in case of alkenyl) should induce charge transfer between the molecules and the Si slab, because of overlap between the π-orbitals of the double bond and the Si surface orbitals, as will be discussed further. We can speculate that the reason for the lack of variation in experimental effective electron affinities is that the combination of all of the above-mentioned factors leads to accidental cancellation of effects, resulting in work function values that are the same within the ±0.1 eV experimental error. This issue is currently being studied further. In the following, we will use the experimental effective electron affinity in analyzing the charge transport.

On the basis of the effective electron affinity, extracted with the aid of eq 1, ϕ_b is predicted to be 0.9 ± 0.1 eV at the Hg/organic molecular monolayer/n-Si junction. This large value explains why the presence of the monolayer at the interface transforms the electrical behavior of the Si−H/Hg junction from Ohmic to rectifying. All these results are summarized in the band diagram of MD n-Si surface, modified with an organic monolayer, before (left) and after (right) contact with Hg (Figure 6).

On the basis of reverse bias $C-V$ and temperature-dependent $J-V$ measurements on MD n-Si/alkyl monolayer/Hg junctions, it was reported that, in contact with a Hg drop, the molecularly modified Si is strongly inverted and that transport across these junctions is minority carrier-controlled.[9,48]

Our $J-V$ and UPS results on alkenyl monolayers indicate that with alkenyl monolayers also the MD n-Si in such MOMS junctions is inverted. The reverse bias $C-V$ measurements on MD n-Si/alkenyl monolayer/Hg junctions yielded results, identical to those for n-Si/alkyl monolayer/Hg ones (see Supporting Information). In addition, we found for the alkenyl monolayers a built-in potential (Ψ_{bi}), doping density (N_D), and barrier height of 0.62 ± 0.03 eV, (8 ± 1) × 10^{14} cm^{-3}, and 0.89 ± 0.03 eV, respectively.[57] For the MD n-Si used here (doping density of N_D ~10^{15} cm^{-3}), the strong inversion potential (Ψ_{inv}) is calculated to be 0.58 eV,[20] i.e., all the junctions on MD n-Si studied here are strongly inverted, minority carrier-controlled

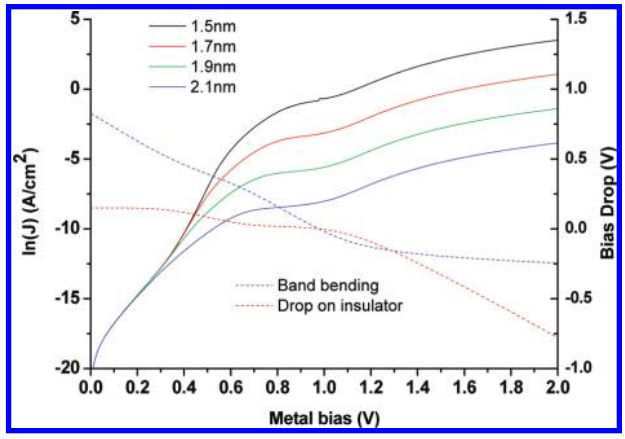

Figure 7. Calculated dependences of $J-V$ curves (solid lines) on monolayer thickness (1.5, 1.7, 1.9, and 2.1 nm), as well as the calculated dependences of the semiconductor band bending (top-dashed, blue) and voltage drop on the insulator (bottom-dashed, red) on the applied bias, for a 2.1-nm-thick monolayer. Calculations are based on the model of Tarr et al.[30]

junctions, with behavior similar to that of an abrupt, one-sided p^+-n one[30,46] rather than the previously assumed majority carrier thermionic emission controlled one.[8,18,58] $J-V$ characteristics of a p^+-n junction are governed by diffusion of minority carriers in the neutral range of the semiconductor and/or generation-recombination in the SCR.[59] Because both minority carrier diffusion and recombination in the SCR are intrinsic semiconductor-related phenomena, to a first approximation the $J-V$ behavior in this range will not be affected by the type or length of the molecules, beyond their effect to drive the Si into inversion.

As explained elsewhere, from $C-V$ measurements only a lower limit of the built-in potential can be extracted,[9,60] and the "real" value will generally be higher. That "real" value of Ψ_{bi} is important from a technological point of view. An increase in Ψ_{bi} will not change the magnitude of the current density in the minority carrier-controlled range (at a given voltage), but will widen that voltage range (relevant for a photovoltaic effect). Camporese and Pulfrey showed numerically that, for metals with different work functions on the same SC-insulator combination (i.e., junctions with different ϕ_b), the onset of tunneling-limited behavior occurs at different current densities.[61] This implies that, under strong inversion, the monolayer's dipole moment controls the electrical properties of the junction only by varying the voltage range over which the current is semiconductor-limited.

High Forward Bias Range. The results in Figure 5 show that the current density, at voltages where length/type dependence initiates, increases as the thickness of the monolayer decreases. To understand the nature of the transition between low and high forward bias, we start with the simplified MIS tunnel diode model of Tarr et al.[30] and use as the insulator dielectric constant that of the organic monolayer rather than that of SiO_2, as was done in the original calculations (see Table 1 in the Supporting Information).

The results of these simulations are presented in Figure 7. The solid lines are $\ln(J)-V$ curves of the four junctions, with 1.5, 1.7, 1.9, or 2.1 nm insulator thickness, i.e., covering the experimental thickness range of the $C_{12}-C_{18}$ monolayers.

The dashed lines present the semiconductor band bending (top, blue) and the voltage drop over the insulator (bottom, red) as a function of applied voltage. For clarity, we show the computation only for a 2.1-nm-thick monolayer. The results for the thinner monolayers (1.5, 1.7, and 1.9 nm) are almost identical to those for the 2.1 nm one with only slight differences in the 0.6−1.2 V transition range. Below 0.6 V, the voltage drop over the insulator is close to constant and negligible, while most of the applied bias falls across the SC, reducing the band bending. Over this range, the current is completely semiconductor-limited and independent of the insulator thickness. In the intermediate 0.6−1.2 V bias range, the applied bias falls across both the SC and the insulator. Over this range, the current starts to level off with increasing bias. Above 1.2 V, the bias that falls over the semiconductor saturates, and any additional bias falls across the insulator. In this regime, there is no significant band-bending left in the semiconductor (semiconductor surface is in accumulation), and transport is dominated by tunneling across the insulator.

Over the intermediate voltage range, the current is extremely sensitive to the molecular properties of the monolayer, i.e., the monolayer width and the surface state density.[46] In this range, the C_{18} and C_{16} $J-V$ curves of alkyl and alkenyl monolayers are different and the current densities of the alkenyl junctions are higher than those of the alkyl junctions (Figure 5).

Effect of Series Resistance. Interpretation of the experimental data at high forward bias is complicated by series resistance effects. As the molecules grow shorter, the current increases and so does the effect of the series resistance.

Qualitatively, our experimentally measured $\ln(J)-V$ curves (Figure 5) are in good agreement with the simulation (Figure 7), with a first transition bias at ~0.6 V and a second at ~1.1 V. Figure 8 compares the theoretical and experimental conductance ($dJ/dV = G$)—voltage characteristics (semilog plots) of the Hg/alkyl/MD n-Si junctions (similar curves are obtained with alkenyl monolayers). It is clear that theory and experiment agree at low forward bias, i.e., over the semiconductor-limited bias range. However, they deviate significantly over the transition and high bias ranges.

Theoretically, the transition range is characterized by a local maximum in the conductance, which correlates with the onset of the nonexponential $J-V$ behavior, followed by a local minimum that correlates with the bias for which the semiconductor goes into accumulation. The experimental $G-V$ curve of the n-Si/C_{18}/Hg system shows the theoretically predicted local maximum and minimum; however, these features become less pronounced as the molecules become shorter and vanish for the C_{12} junction. Furthermore, the conductance of the $C_{12}-C_{16}$ systems at 2 V is nearly independent of the molecular length. This implies that the current density at high applied voltage ($V_{app} > 0.6$ V) is limited by series, rather than by the tunneling, resistance.

We estimated experimentally, using Ohm's law, the series resistance, R_S, for the Si−H/Hg junction in our measurement setup to be ~30 ohm over the 1.5−2 V bias range. The measured current at 0.6 V, the onset of the transition range, was 9 μA for the C_{18} and 150 μA for the C_{12} system. Hence, the resistive voltage losses ($= I \times R_S$) are 0.26 mV and 4.6 mV, respectively. Although the voltage drop over R_S is ~15 times larger in the case of the C_{12} than for the C_{18} system, it is remarkable that a ~5 mV voltage drop can have such an effect on the charge transport characteristics, while the applied bias is 130 times larger (600 mV). The reason is that, up to the transition between semiconductor and tunneling limited region, the bias drop is mainly on the depletion layer of the SC (Figure 7 dashed, blue line), while the bias drop on the insulator is negligible (Figure 7 dashed, red line). Therefore, a 5 mV bias

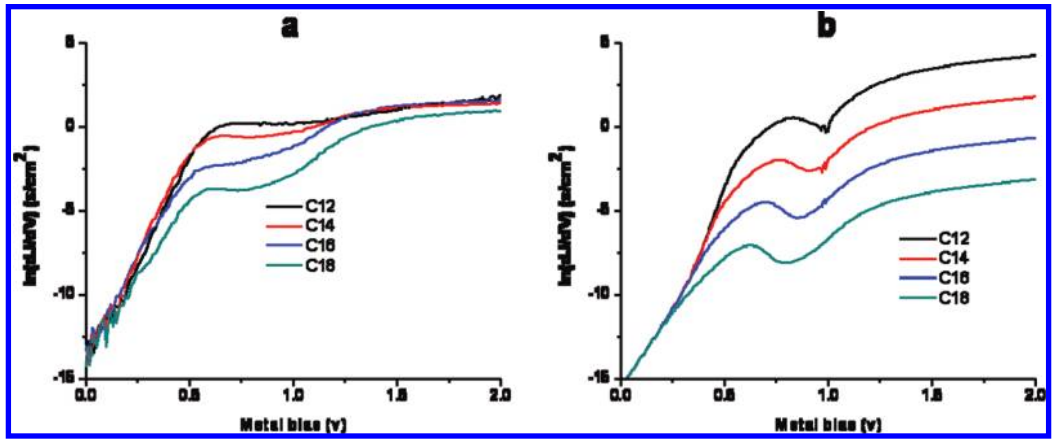

Figure 8. Comparison between the dependence of experimental (a) and simulated (b) conductance ($G = dJ/dV$) as a function of applied bias on Hg/alkyl/MD n-Si junctions. The widths used in the simulations (1.5, 1.7, 1.9, and 2.1 nm) correspond to the experimentally measured thicknesses of the alkyl monolayers (C_{12}, C_{14}, C_{16}, and C_{18}).

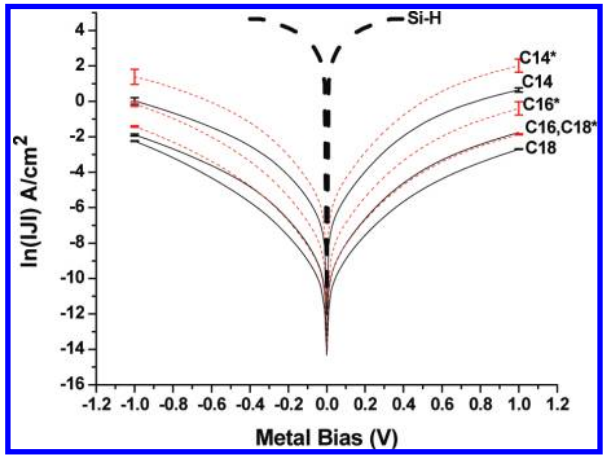

Figure 9. Ln(|J|)−V curves of HD n-Si/monolayer/Hg of both alkenes (black - solid) and alkynes (red - dashed lines) of several lengths (14, 16, and 18 carbon chains) and of freshly etched n-Si-H/Hg (----). Bias is applied to the Hg. Si is grounded. Results are logarithmic average of at least 7 different junctions with a scan rate of 20 mV/s. The error bars represent standard deviations, typically less than 5% of the measured current.

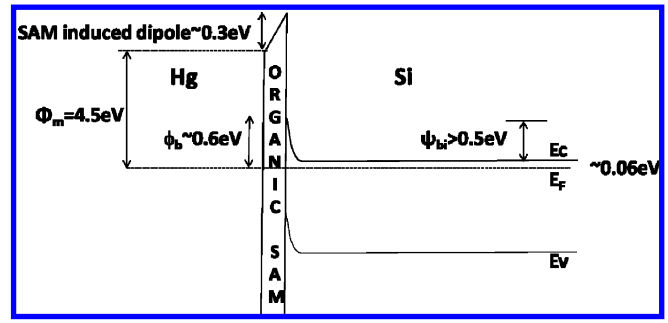

Figure 10. Band diagram of organic monolayer/HD n-Si structure after contact with Hg, where Ψ_{bi} is the built-in potential, measured as band bending, ϕ_b is the barrier for transport (calculated), and Φ_m is the Hg work function.

drop on series resistance is small compared to the total applied bias, but is significant compared to the actual bias drop on the insulator.

So far, we have presented an example for two different monolayers on Si that exhibit identical electrical properties over most of the examined bias range. This identical behavior originates from the inverted Si surface, which is induced by the molecular dipole (at reverse and low forward bias) and series resistance (at high forward bias). Sensitivity to molecular transport properties (e.g., length) was expressed only over a small part of the bias range and over the transition range, where neither the semiconductor nor the molecular contributions can be neglected. Therefore, although a length-dependent current is observed for MD-junctions, quantitative analysis of molecularly controlled transport[8,14,58,62,63] (e.g., extracting the current decay parameter, β) is ill-defined at this stage and might lead to misleading conclusions. This problem can be overcome by using HD Si as is described in the next section.

Electrical Properties of MOMS Junctions on HD n-Si. Figure 9 shows the averaged ln(|J|)−V curves of junctions with either alkyl (black) or alkenyl monolayers (red) on HD n-Si(111), as well as the J−V curve of such a junction with freshly etched H−Si(111) (dashed). The chain length is given as the number of carbons and an asterisk denotes the alkenyl monolayers.

Compared to MOMS junctions on MD n-Si (Figure 5), we note three important features: (1) The reverse bias (negative on the metal) current density is comparable to the forward bias current density. Furthermore, the ln(J)−V characteristic in the forward bias (positive bias on the metal) is not exponential as expected for diode-like transport (i.e., it is not linear in Figure 9). (2) The current density is length-dependent over all of the measured bias range. (3) The current density of an alkenyl monolayer junction is higher than that of the analogue alkyl monolayer over the whole measured bias range.

Rectifying vs Nonrectifying Behavior. The characterizations of our monolayers (vide supra) on Si with different doping levels show no or at most a marginal effect of the doping level on the monolayer structure. Therefore, we ascribe the transition from rectifying (MD n-Si, Figure 5) to nonrectifying behavior (HD n-Si, Figure 9) mainly to the electronic effects of the doping density of the Si.

First, while the strong inversion potential for MD n-Si is 0.58 eV, it is >1 eV[20] for HD n-Si at room temperature. CPD measurements indicated that the work function of the HD samples is ~4.0 ± 0.1 eV, which can be compared to 4.25 ± 0.1 eV for freshly etched n-Si-H.[22] On the basis of the nominal doping density ($N_d \sim 10^{19}$ cm^{-3}),$|E_V - E_F|_{Bulk}$ is about 1 eV. Hence, the effective electron affinity is expected to be ~4 eV, and according to the Schottky limit (eq 1) under a Hg contact, the barrier height for charge transport and the surface potential of the HD n-Si are expected to be 0.6 and 0.5 eV, respectively. All these results are summarized in the band diagram for the HD n-Si junction (Figure 10).

This means that, in contrast to the surface of MD n-Si under Hg, the surface of HD n-Si is not inverted and charge transport

is majority carrier-controlled.[46] Nevertheless, a potential barrier of 0.6 eV is expected to induce a stronger asymmetry in the $J-V$ curves than that observed in Figure 9. There are three different mechanisms that can lead to nonrectifying $J-V$ curves on the HD n-Si substrate: (1) interfacial layer-induced barrier lowering, i.e., the potential drop across the insulating layer makes the equilibrium barrier height lower than it would be without the layer;[21,64] (2) tunneling through the barrier, i.e., with increasing doping density thermionic field emission becomes more significant, due to the narrower depletion layer width; (3) field dependence of the barrier height, which can arise from the effect of the image force, which in turn depends strongly on doping density, or from the effect of trapped charges in interface states and/or in an interfacial layer (which can increase with doping density).[21]

The nonrectifying $J-V$ curves indicate that, in contrast to what is the case for MD n-Si, the internal barrier in the HD n-Si is quite small and the $J-V$ characteristics are dominated mainly by the presence of the monolayer. Indeed, both the length dependence within a single type of monolayer ($C_{14}-C_{18}$) and the differences in current density between monolayer types (alkyl vs alkenyl) with identical number of carbons indicate that this is the case (Figure 9).

J−V Length Dependence. It is clear from Figure 9 that for alkyl monolayers the decrease in current between C_{14} and C_{16} is much larger than that between C_{16} and C_{18}. This result is very reproducible, correlates with the ellipsometry measurements (Table 1) and agrees with previously reported results on a similar system.[65] The same phenomenon is also seen, but less pronounced, for the alkenyl monolayers. A possible reason might be a difference in structure between longer (C_{16} and C_{18}) and shorter monolayers, consistent with the ellipsometric thicknesses of the monolayers. Such difference will cause an error in the extraction of length-dependent parameters. Still, even with such errors, the approximate values that we can get from calculating these parameters can give an idea of the main differences between alkyl and alkenyl monolayers. For this purpose, we briefly summarize the expected length effect on electronic transport.

Transport of electrons through a saturated molecular system is commonly considered an elastic scattering problem of free electrons (described by the Landauer relation),[52,66,67] where the tunneling probability through the barrier, introduced by the molecule, decays exponentially with the length. In this model, the conductance of a single channel (G) is described as[4,68,69]

$$G = G_C \exp(-\beta l) \qquad (2)$$

where l is the length of the molecule, β is the length-decay parameter, and G_C is the contact conductance. The averaged reported β value for transport across saturated alkyl chains is $0.9 \pm 0.2/CH_2$.[4] Here, we extracted β values of $0.9/CH_2$ for the alkyls and $0.95/CH_2$ for the alkenyls at an applied bias of 0.2 V with a fitting error of 0.2 (see Supporting Information), similar to the reported average values. The relative similarity between alkyl and alkenyl monolayers is expected, as only one bond out of 14 (or more) in these chains is changed. However, because the double bond is close to the substrate, its effect is more likely to be felt in the coupling to the contact than in the transmission through the molecules. This result is consistent with the results presented by Engelkes et al., where variations in the metal work function for MIM junctions of alkyl thiols or dithiols had a pronounced effect on the net current, but not on the length decay (β).[70] In addition, Nesher et al., considering transport through alkyls on GaAs,[63] and Thieblemont et al., considering Si−O vs Si−C bound alkyls on Si,[58] concluded that the charge-transport properties of saturated alkyl chain MOMS with different anchoring groups differ mainly in the molecule−substrate coupling. In the case of the work by Nesher et al, we can also derive β and G_C values (see next section) from their data ($0.65/CH_2$ and 2.5×10^{-6} G_o, respectively).

Alkyl vs Alkenyl−the Effect of Electrode−Monolayer Electrical Coupling. While β is similar for the two types of monolayers, the values for G_C, which are determined by the molecule-electrode coupling strength, are different. Assuming that every molecule presents a single conductance channel and that the footprint of a single molecule is a ~ 0.2 nm^2/molecule,[61,67,71] we find that the contact conductances are $(4.7 \pm 1.3) \times 10^{-7}$ G_0 (with $G_0 \equiv (2q^2)/(h) = 77.4$ μS) for alkyl and $(13 \pm 8) \times 10^{-7}$ G_0 for alkenyl monolayers. As noted earlier for alkyl chain (and other molecular) junctions, the experimental G_C values are much lower than G_0[48] and are sensitive to interface chemistry.[69,70,72,73] One possible factor that reduces G_C is the limited density of states available for transport in a semiconductor (cf. also for GaAs as mentioned above[65]), compared to a metal. However, also in metal/molecule/metal junctions G_C is much smaller than G_0. Akkerman and De Boer[4] compiled the conductance for a large number of metal/alkyl/metal junctions and correlated it with the molecular length. The intercept of their fit reveals $G_C = 2.4 \times 10^{-4}$ G_0 for one (bottom electrode) and 1.6×10^{-2} G_0 for two chemical contacts (bottom and top), respectively, in qualitative agreement with earlier reports by Selzer et al.[74] and Salomon et al.[67] The higher contact conductance for the two chemi-contact junction can be ascribed to enhanced coupling (orbital overlap) between the electrode and molecules, if there is a covalent bond between them. Furthermore, the contact conductance is sensitive to the metal of the electrode and was found to vary by up to 4 orders of magnitude, depending on whether Ag, Au, or Pt served as the electrode,[70] with an exponential dependence on the metal's work function. This suggests that the coupling term depends on the energy difference between the electrode's Fermi level and the relevant molecular levels.[70,75] Such dependence is readily understood if we consider that the molecule−electrode coupling leads to new levels. The original LUMO and HOMO of the molecules should, at the interface, be replaced by the LUSO and HOSO (lowest unoccupied and highest occupied SYSTEM orbitals), which will be closer to the semiconductor band edges than the HOMO and LUMO of the isolated molecules or free monolayer.[37] These orbitals will influence tunneling, as well as hopping transport. In addition, tunneling will depend strongly on states that result from the interactions between the conduction band and valence band levels and the molecular levels, the so-called "induced density of interface states", IDIS,[76] which will be the energy levels closest to the SC band edges.

To further examine the Si−organic chain coupling, we performed a DFT calculation of the alkyl and alkenyl systems. The local densities of states of the two systems are shown as a function of position (in the direction perpendicular to the surface) and energy in Figure 11. Clearly, Si-related states are found to extend further into the molecular region in the alkenyl case (up to the third carbon) than in the alkyl case (up to the second carbon). In the latter case, the dominant states contributing to the extension of the Si states are of the IDIS type.[37] In the alkenyl case,they are a combination of IDIS and π-orbitals. These π-orbitals originate from the double bond between the first carbon, found closest to the surface, and the second carbon. This is due to the overlap between the unbound allowed Si

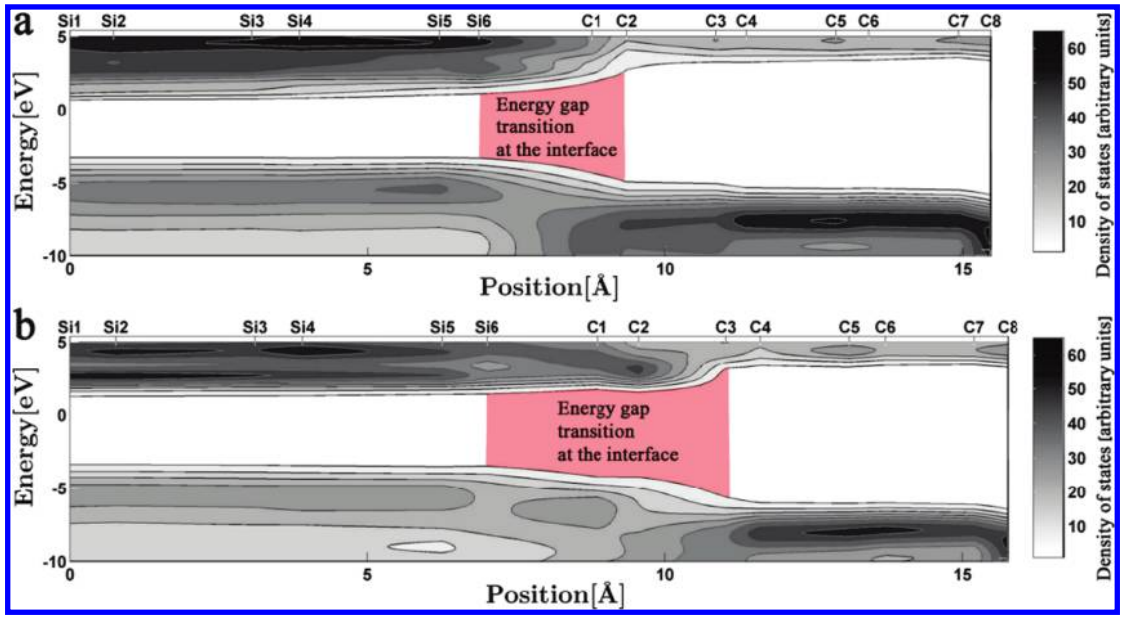

Figure 11. Contour maps of the local density of states for (a) alkyl and (b) alkenyl monolayers on Si(111).[77] The interfacial transition region is emphasized in red.

surface levels and the C═C π-bonding levels of the isolated alkenyl molecule, i.e., the HOMO−LUMO gap of the double bond in the isolated molecule is similar to the Si band gap. The extended nature of Si-related states is consistent with enhanced coupling between the Si substrate and the alkenyl SAM, relative to that of the alkyl SAM. Hence, due to molecule−semiconductor coupling even just one double bond in a long alkyl chain can affect the electrical characteristics of a MOMS device, as long as the effect of the internal barrier of the SC does not dominate transport (as is the case with MD Si).

Conclusions

By comparing alkyl and alkenyl self-assembled monolayers that differ only by a double bond adjacent to the surface (Figure 1), on two different n-Si substrates (moderately and heavily doped) we find that with moderately doped Si the combination of the relatively wide space charge region of the Si, together with the large surface dipole layer, induced by the molecular monolayer, creates a minority carrier-controlled junction. Transport across such a junction is indifferent to the charge-transport properties of the attached monolayer at reverse and low forward bias and, in our case, is affected by series resistance at high forward bias.

For highly doped Si, the internal SC barrier decreases so as to become less significant, compared to the barrier posed by the molecular monolayer. As a result, we cannot observe effects of the double bond near the surface and find that the main influence is to enhance Si−molecule coupling, which increases the contact conductance and by that increases the current density at a given applied bias.

If we take a more general view, our results show that molecular features, i.e., the surface dipole, induced by the molecules and the molecular effect on the charge transport barrier, are expressed differently for different doping levels of otherwise identical semiconductor substrates.

While the electrical properties of MOMS junctions on a moderately doped semiconductor are strongly dependent on the surface dipole that is induced by the molecules, the electrical properties of a similar junction on a heavily doped semiconductor are very sensitive to the charge transport barrier that is strongly influenced by the molecule.

Thus, the electrical properties of MOMS junctions on HD and MD semiconductor substrates are complementary and present a microlaboratory to study a given molecular system.

Acknowledgment. D.C. and A.K. thank the US-Israel Binational Science Foundation, D.C. and L.K. thank the Israel Science Foundation, ISF, through its Converging Technology and Centre of Excellence programs, L.K. thanks the Lise Meitner - Minerva Center for Computational Chemistry, and D.C. also thanks the Monroe and Marjorie Burk Fund for Alternative Energy Studies for partial support. At the Weizmann Institute, this work was made possible in part by the historic generosity of the Harold Perlman family. A.K. thanks the National Science Foundation (DMR-0705920) and the Princeton MRSEC of the National Science Foundation (DMR-0819860). H.Z. thanks NanoNed, funded by the Dutch Ministry of Economic Affairs (project WSC.6972) for financial support. O.Y. thanks the Azrieli Foundation for the award of an Azrieli Fellowship. D.C. holds the Sylvia and Rowland Schaefer Chair in Energy Research.

Supporting Information Available: Additional data as described in the text. This material is available free of charge via the Internet at http://pubs.acs.org.

References and Notes

(1) Heath, J.; Ratner, M. A. *Physics Today* **2003**, p. 43.
(2) Aviram, A.; Ratner, M. A. *Molecular Electronics: Science and Technology*; The Annals of the New York Academy of Sciences; New York Academy of Sciences: New York, 1998; Vol. 852.
(3) Ulman, A. *An introduction to ultrathin organic films: from Langmuir-Blodgett to self assembly*; Boston, MA, 1991.
(4) Akkerman, H. B.; de Boer, B. *J. Phys.: Condens. Matter* **2008**, *20*, 013001.
(5) Guisinger, N. P.; Greene, M. E.; Basu, R.; Baluch, A. S.; Hersam, M. C. *Nano Lett.* **2004**, *4*, 55–59.
(6) Wang, W.; Scott, A.; Gergel-Hackett, N.; Hacker, C. A.; Janes, D. B.; Richter, C. A. *Nano Lett.* **2008**, *8*, 478–484.
(7) Adina, S.; David, B. J.; Chad, R.; Mark, A. R. *App. Phys. Lett.* **2007**, *91*, 033508.

(8) Salomon, A.; Böcking, T.; Seitz, O.; Markus, T.; F., A.; Chan, C.; Zhao, W.; Cahen, D.; Kahn, A. *Phys. Rev. Lett.* **2005**, *95*, 266807.
(9) Yaffe, O.; Scheres, L.; Puniredd, S. R.; Stein, N.; Biller, A.; Lavan, R. H.; Shpaisman, H.; Zuilhof, H.; Haick, H.; Cahen, D.; Vilan, A. *Nano Lett.* **2009**, *9*, 2390–2394.
(10) Buriak, J. M. *Chem. Rev.* **2002**, *102*, 1271–1308.
(11) Ciampi, S.; Böcking, T.; Kilian, K. A.; James, M.; Harper, J. B.; Gooding, J. J. *Langmuir* **2007**, *23*, 9320–9329.
(12) Scheres, L.; Arafat, A.; Zuilhof, H. *Langmuir* **2007**, *23*, 8343–8346.
(13) Puniredd, S. R.; Assad, O.; Haick, H. *J. Am. Chem. Soc.* **2008**, *130*, 13727–13734.
(14) Salomon, A.; Böcking, T.; Seitz, O.; Markus, T.; Amy, F.; Chan, C.; Zhao, W.; Cahen, D.; Kahn, A. *Adv. Mater.* **2007**, *19*, 445.
(15) Miramond, C.; Vuillaume, D. *J. Appl. Phys.* **2004**, *96*, 1529–1536.
(16) Ralf, H.; Rainer, F.; Bengt, J.; Wolfram, J.; Lauren, J. W.; Lewis, N. *Phys. Rev. B* **2005**, *72*, 045317.
(17) Maldonado, S.; Plass, K. E.; Knapp, D.; Lewis, N. S. *J. Phys. Chem. C* **2007**, *111*, 17690–17699.
(18) Faber, E. J.; de Smet, L.; Olthuis, W.; Zuilhof, H.; Sudhölter, E. J.; Bergveld, P.; Van den Berg, A. *ChemPhysChem* **2005**, *6*, 2153–2166.
(19) Kar, S. *Appl. Surf. Sci.* **2006**, *252*, 3961.
(20) Sze, S. M.; Ng, K. K. *Physics of Semiconductor Devices*, 3rd ed.; John Wiley & Sons, Inc.: New York, 2007.
(21) Rhoderick, E.; Williams, R. *Monographs in Electrical and Electronic Engineering. Metal-Semiconductor Contacts*, 2nd ed.; Clarendon Press: Oxford, 1988.
(22) It seems that the dipole effect of the adsorbed molecular monolayer on heavily doped Si is smaller than on moderately doped Si. A quantitative study of this issue is currently in progress.
(23) Rampi, M. A.; Whitesides, G. M. *Chem. Phys.* **2002**, *281*, 373.
(24) Mann, B. *J. Appl. Phys.* **1971**, *42*, 4398.
(25) Liu, Y.; Yu, H. *ChemPhysChem* **2002**, *3*, 799–802.
(26) Seitz, O.; Böcking, T.; Salomon, A.; Gooding, J. J.; Cahen, D. *Langmuir* **2006**, *22*, 6915–6922.
(27) Scheres, L.; Giesbers, M.; Zuilhof, H. *Langmuir* **2010**, *26*, 4790–4795.
(28) Petroleum ether with a boiling point between 40 and 60 °C.
(29) Brunner; Mayer, U.; Hoffman, *Appl. Spectrosc.* , *51*, 209–217.
(30) Tarr, N. G.; Pulfrey, D. L.; Camporese, D. S. *IEEE Trans. Electron Devices* **1983**, *30*, 1760.
(31) Makov, G.; Payne, M. C. *Phys. Rev. B* **1995**, *51*, 4014.
(32) Natan, A.; Kronik, L.; Shapira, Y. *App. Surf. Sci.* **2006**, *252*, 7608–7613.
(33) Kresse, G.; Furthmüller, J. *Phys. Rev. B* **1996**, *54*, 11169.
(34) Gross, E. K. U.; Dreizler, R. M. *Density functional theory*; Springer: Berlin, 1995.
(35) Magid, I.; Burstein, L.; Seitz, O.; Segev, L.; Kronik, L.; Rosenwaks, Y. *J. Phys. Chem. C* **2008**, *112*, 7145–7150.
(36) Amy, F.; Chan, C. K.; Zhao, W.; Hyung, J.; Ono, M.; Sueyoshi, T.; Kera, S.; Nesher, G.; Salomon, A.; Segev, L.; Seitz, O.; Shpaisman, H.; Scholl, A.; Haeming, M.; Böcking, T.; Cahen, D.; Kronik, L.; Ueno, N.; Umbach, E.; Kahn, A. *J. Phys. Chem. B* **2006**, *110*, 21826–21832.
(37) Segev, L.; Salomon, A.; Natan, A.; Cahen, D.; Kronik, L.; Amy, F.; Chan, C. K.; Kahn, A. *Phys. Rev. B* **2006**, *74*, 165323–6.
(38) van Alem, K.; Lodder, G.; Zuilhof, H. *J. Phys. Chem. A* **2002**, *106*, 10681–10690.
(39) Faber, E. J.; Sparreboom, W.; Groeneveld, W.; Smet, L. C. P. M. D.; Bomer, J.; Olthuis, W.; Zuilhof, H.; Sudhölter, E. J. R.; Bergveld, P.; Berg, A. V. D. *ChemPhysChem* **2007**, *8*, 101–112.
(40) Sun, Q.; de Smet, L.; van Lagen, B.; Giesbers, M.; Thune, P. C.; van Engelenburg, J.; de Wolf, F. A.; Zuilhof, H.; Sudhölter, E. J. R. *J. Am. Chem. Soc.* **2005**, *127*, 2514–2523.
(41) Porter, M. D.; Bright, T. B.; Allara, D. L.; Chidsey, C. E. D. *J. Am. Chem. Soc.* **1987**, *109*, 3559–3568.
(42) Snyder, R. G.; Strauss, H. L.; Elliger, C. A. *J. Phys. Chem.* **1982**, *86*, 5145–5150.
(43) Wallart, X.; Henry de Villeneuve, C.; Allongue, P. *J. Am. Chem. Soc.* **2005**, *127*, 7871–7878.
(44) Allongue, P.; Henry de Villeneuve, C.; Morin, S.; Boukherroub, R.; Wayner, D. D. M. *Electrochim. Acta* **2000**, *45*, 4591–4598.
(45) Ramonda, M.; Dumas, P.; Salvan, F. *Surf. Sci.* **1998**, *411*, L839–L843.
(46) Green, M. A.; King, F. D.; Shewchun, J. *Solid-State Electron.* **1974**, *17*, 551.
(47) The effective electron affinity is given by $\chi_{eff} = \Phi_{SC} - (E_g - |E_v - E_f|_s)$, where Φ_{SC} is the work function of the Si + molecules substrate, E_g is the Si band gap, and $|E_v - E_f|_s$ is the difference between the energy level of the valence band (E_v) and the Fermi level (E_f) at the surface. Both Φ_{SC} and $|E_v - E_f|_s$ can by directly measured either by UPS or by combined CPD/SPV (surface photovoltage) measurement. See ref 51, Figure 4 p 18.
(48) Vilan, A.; Yaffe, O.; Biller, A.; Salomon, A.; Kahn, A.; Cahen, D. *Adv. Mater.* **2010**, *22*, 140–159.
(49) Brillson, L. *Surf. Sci. R.* **1982**, *2*, 123–326.
(50) Wittmer, M.; Freeouf, J. L. *Phys. Rev. Lett.* **1992**, *69*, 2701.
(51) Hunger, R.; Fritsche, R.; Jaeckel, B.; Jaegermann, W.; Webb, L. J.; Lewis, N. S. *Phys. Rev. B* **2005**, *72*, 045317.
(52) Heimel, G.; Romaner, L.; Zojer, E.; Bredas, J. *Acc. Chem. Res.* **2008**, *41*, 721–729.
(53) Jaeckel, B.; Hunger, R.; Webb, L. J.; Jaegermann, W.; Lewis, N. S. *J. Phys. Chem. C* **2007**, *111*, 18204–18213.
(54) Natan, A.; Kronik, L.; Haick, H.; Tung, R. *Adv. Mater.* **2007**, *19*, 4103–4117.
(55) Kronik, L.; Shapira, Y. *Surf. Sci. Rep.* **1999**, *37*, 1–206.
(56) Walker, P.; Tarn, W. H. *CRC handbook of metal etchants*; CRC Press: Boca Raton, 1990.
(57) The error represents the standard deviation between the samples.
(58) Thieblemont, F.; Oliver, O.; Vilan, A.; Cohen, H.; Salomon, E.; Kahn, A.; Cahen, D. *Adv. Mater.* **2008**, *20*, 3931–3936.
(59) Sah, C. T.; Noyce, R. N.; Shockley, W. *Proc. IRE* **1957**, *45*, 1228.
(60) Shewchun, J.; Green, M. A.; King, F. D. *Solid-State Electron.* **1974**, *17*, 563.
(61) Camporese, D. S.; Pulfrey, D. L. *J. Appl. Phys.* **1985**, *57*, 373–376.
(62) Salomon, A.; Böcking, T.; Gooding, J. J; Cahen, D. *Nano Lett.* **2006**, *6*, 2873−2876.
(63) Nesher, G.; Shpaisman, H.; Cahen, D. *J. Am. Chem. Soc.* **2007**, *129*, 734–735.
(64) Provided that there is no charge contained in the layer.
(65) Furuhashi, M.; Omura, A.; Yamashita, Y.; Mukai, K.; Yoshinobu, J.; Akagi, K.; Tsuneyuki, S. *Jpn. J. Appl. Phys.* **2009**, *48*, 055003.
(66) Adams, D. M.; Brus, L.; Chidsey, C. E. D.; Creager, S.; Creutz, C.; Kagan, C. R.; Kamat, P. V.; Lieberman, M.; Lindsay, S.; Marcus, R. A.; Metzger, R. M.; Michel-Beyerle, M. E.; Miller, J. R.; Newton, M. D.; Rolison, D. R.; Sankey, O.; Schanze, K. S.; Yardley, J.; Zhu, X. *J. Phys. Chem. B* **2003**, *107*, 6668–6697.
(67) Salomon, A.; Cahen, D.; Lindsay, S.; Tomfohr, J.; Engelkes, V. B.; Frisbie, C. D. *Adv. Mater.* **2003**, *15*, 1881–1890.
(68) Magoga, M.; Joachim, C. *Phys. Rev. B* **1997**, *56*, 4722.
(69) Chen, F.; Li, X.; Hihath, J.; Huang, Z.; Tao, N. *J. Am. Chem. Soc.* **2006**, *128*, 15874–15881.
(70) Engelkes, V. B.; Beebe, J. M.; Frisbie, C. D. *J. Am. Chem. Soc.* **2004**, *126*, 14287–14296.
(71) York, R. L.; Nacionales, D.; Slowinski, K. *Chem. Phys.* **2005**, *319*, 235.
(72) Monnell, J. D.; Stapleton, J. J.; Dirk, S. M.; Reinerth, W. A.; Tour, J. M.; Allara, D. L.; Weiss, P. S. *J. Phys. Chem. B* **2005**, *109*, 20343–20349.
(73) Yoo, H.; Choi, J.; Wang, G.; Kim, T.; Noh, J.; Lee, T. *J. Nanosci. Nanotechnol.* **2009**, *9*, 7012–7015.
(74) Selzer, Y.; Salomon, A.; Cahen, D. *J. Phys. Chem. B* **2002**, *106*, 10432–10439.
(75) Quinn, J. R.; Foss, F. W.; Venkataraman, L.; Breslow, R. *J. Am. Chem. Soc.* **2007**, *129*, 12376–12377.
(76) Vazquez, H.; Dappe, Y. J.; Ortega, J.; Flores, F. *J. Chem. Phys.* **2007**, *126*, 144703.
(77) The unoccupied levels have been rigidly shifted so as to yield the correct alkyl chain gap (as inferred from a combination of UPS and IPES). As a consequence, the silicon gap is larger than the experimental one.

JP101656T